Accepted Manuscript

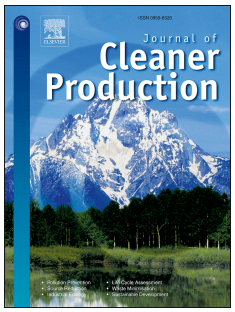

Synergistic effects of activated carbon and nano-zerovalent copper on the performance of hydroxyapatite-alginate beads for the removal of As^{3+} from aqueous solution

Jibran Iqbal, Noor S. Shah, Murtaza Sayed, Muhammad Imran, Nawshad Muhammad, Fares M. Howari, Sara A. Alkhoori, Javed Ali Khan, Zia Ul Haq Khan, Amit Bhatnagar, Kyriaki Polychronopoulou, Issam Ismail, Mohammad Abu Haija

PII: S0959-6526(19)32293-0

DOI: https://doi.org/10.1016/j.jclepro.2019.06.316

Reference: JCLP 17485

To appear in: *Journal of Cleaner Production*

Received Date: 28 March 2019

Revised Date: 26 June 2019

Accepted Date: 28 June 2019

Please cite this article as: Iqbal J, Shah NS, Sayed M, Imran M, Muhammad N, Howari FM, Alkhoori SA, Khan JA, Haq Khan ZU, Bhatnagar A, Polychronopoulou K, Ismail I, Haija MA, Synergistic effects of activated carbon and nano-zerovalent copper on the performance of hydroxyapatite-alginate beads for the removal of As^{3+} from aqueous solution, *Journal of Cleaner Production* (2019), doi: https://doi.org/10.1016/j.jclepro.2019.06.316.

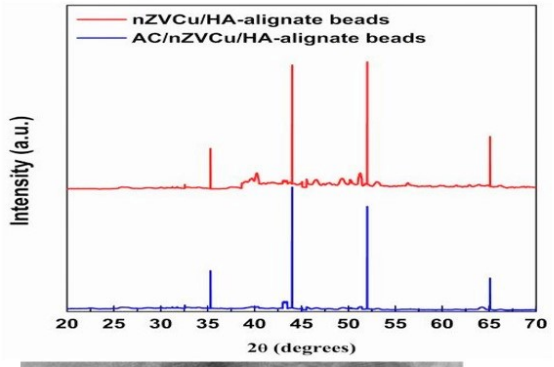

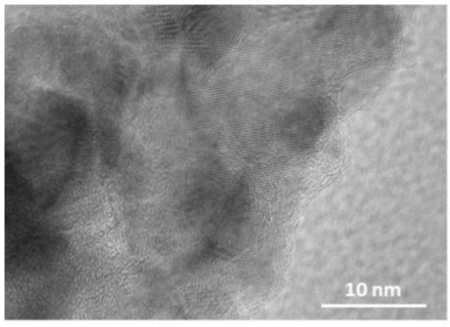

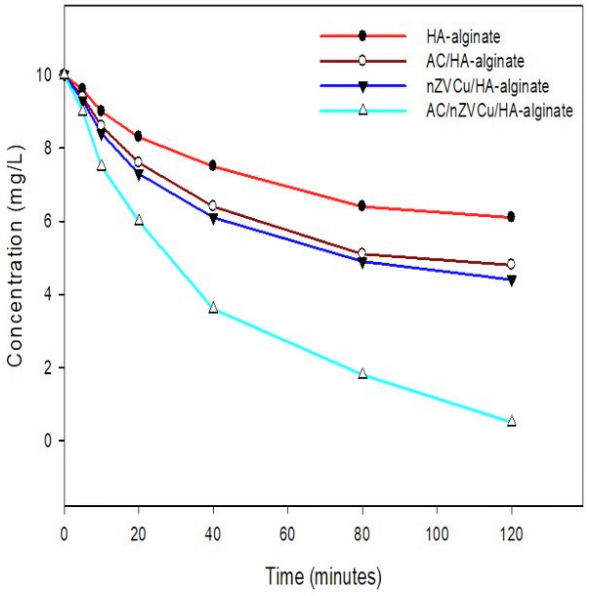

Synergistic effects of activated carbon and nano-zerovalent copper on the performance of hydroxyapatite-alginate beads for the removal of As^{3+} from aqueous solution

Jibran Iqbal[1], Noor S. Shah[2, *], Murtaza Sayed[3], Muhammad Imran[2], Nawshad Muhammad[4], Fares M. Howari[1], Sara A. Alkhoori[1], Javed Ali Khan[3], Zia Ul Haq Khan[3], Amit Bhatnagar[5], Kyriaki Polychronopoulou[6,7], Issam Ismail[8], Mohammad Abu Haija[9]

[1]College of Natural and Health Sciences, Zayed University, P.O. Box 144534, Abu Dhabi, United Arab Emirates

[2]Department of Environmental Sciences, COMSATS University Islamabad, Vehari Campus 61100, Pakistan

[3]Radiation Chemistry Laboratory, National Centre of Excellence in Physical Chemistry, University of Peshawar, Peshawar 25120, Pakistan

[4]Interdisciplinary Research Centre for Biomedical Materials, COMSATS University Islamabad, Lahore Campus 54000, Pakistan

[5]Department of Environmental and Biological Sciences, University of Eastern Finland, P.O. Box 1627, FI-70211, Kuopio, Finland

[6]Department of Mechanical Engineering, Khalifa University of Science and Technology, Abu Dhabi, UAE, P.O. Box: 127788, United Arab Emirates

[7]Center for Catalysis and Separation, Khalifa University of Science and Technology, Abu Dhabi, UAE, P.O. Box: 127788, United Arab Emirates

[8]Department of Chemical Engineering, Khalifa University of Science and Technology, Abu Dhabi, UAE, P.O. Box: 127788, United Arab Emirates

[9]Department of Chemistry, Khalifa University of Science and Technology, Abu Dhabi, United Arab Emirates

Corresponding Author:

Noor S. Shah: samadchemistry@gmail.com

(Tel: +92-334-9158516)

Abstract

In this study, activated carbon (AC) and nano-zerovalent copper (nZVCu) functionalized hydroxyapatite (HA) and alginate beads are synthesized and used for the removal of As^{3+} from aqueous solution. The characterization by X-ray diffraction, scanning electron microscopy, X-ray energy dispersive spectroscopy, X-ray photoelectron spectroscopy, transmission electron microscopy, high resolution transmission electron microscopy, BET surface area analysis, thermogravimetric analysis, and Fourier transform infrared spectroscopy revealed successful formation of the AC/nZVCu/HA-alginate, nZVCu/HA-alginate, AC/HA-alginate, and HA-alginate beads. The scanning electron microscopy and surface analysis revealed the prepared beads to be highly mesoporous which led to the maximum adsorption of As^{3+}, i.e., 13.97, 29.33, 30.96, and 39.06 mg/g by HA-alginate, AC/HA-alginate, nZVCu/HA-alginate, and AC/nZVCu/HA-alginate beads, respectively. The thermogravimteric analysis showed the nZVCu/HA-alginate beads to be highly stable while the AC composite beads as the least stable to heat treatment. The HA-alginate beads achieved 39% removal of As^{3+}, however, removal efficiency was promoted to 95% by coupling AC and nZVCu with HA-alginate beads at a reaction time of 120 min. The removal of As^{3+} by the prepared AC & nZVCu coupled HA-alginate beads was promoted with increasing $[As^{3+}]_0$ and [AC/nZVCu/HA-alginate]$_0$. The pH of aqueous solution significantly influenced the removal of As^{3+} by AC/nZVCu/HA-alginate beads and maximum removal was achieved at pH 5.8. Freundlich adsorption isotherm and *pseudo-second-order* kinetic models were found to best fit the removal of As^{3+} by the synthesized beads. The high performance of

AC/nZVCu/HA-alginate beads in the removal of As^{3+} even after seven cyclic treatment as well as least leaching of Cu ions into aqueous solution suggest enhanced reusability and stability of HA-alginate beads by coupling with AC and nZVCu. The results suggest that the synthesized beads have good potential for the removal of As^{3+} and other toxic heavy metals from aqueous solutions.

Key Words: As^{3+}; Hydroxyapatite-alginate beads; Activated Carbon; Nano-zerovalent copper; Water treatment.

1. Introduction

Water is an essential entity of universe; however, quality of water is continually being declined by contaminations with foreign substances, both from natural and anthropogenic activities (Sayed et al., 2019; Shah et al., 2019). Among the various water pollutants, heavy metals are considered as the major contributors (Murtaza et al., 2019). Arsenic (As), a globally considered significant cause of environmental cancer mortality, is one of the most prominent heavy metal water contaminants (Martinez et al., 2011; WHO, 2011a). The concentration of As exceeding the maximum acceptable concentration recommended by the World Health Organization (WHO) has been reported in water resources throughout the world (Amini et al., 2008; WHO, 2011b). Arsenic is reported in water resources in both inorganic (i.e., arsenite [As^{3+} and arsenate^{5+}] and organic forms (e.g., monomethylarsonic acid (MMA) and dimethylarsinic acid (DMA)), however, the inorganic form (As^{3+}) is highly toxic and of great environmental concern (Mohan et al., 2007). As^{3+} is reported to cause several short and long term effects on human health and the environment as a whole (Mohan et al., 2007). Owing to serious environmental and health issues, highly vital is to remove As^{3+} from water resources. Various techniques, such as adsorption, coagulation, ion exchange, and reverse osmosis have been used for effective As^{3+} removal from water (Hamayun et al., 2014). Among such techniques, adsorption has been more effective and efficient in As^{3+} removal (Hamayun et al., 2014). Recently, biomaterials are used as an adsorbent that are preferred due to their low cost, easier availability in large quantities, and lower waste management rudiments after use (Lesmana et al., 2009; Nguyen et al., 2013; Li et al., 2018). Among the biomaterials, biopolymers are widely used in water treatment due to their wide range applications, such

as biodegradability and eco-friendly nature (Ahmed et al., 2014). Sodium alginate, a biopolymer with unique properties, such as hydrophilicity, biocompatibility, and non-toxic nature, is selected as source of biomaterial for the removal of As^{3+}. In order to improve its performance, sodium alginate is combined with hydroxyapatite (HA, $Ca_{10}(PO_4)_6(OH)_2$), an inorganic material with high biocompatibility and adsorption capacity. The composite beads of HA and sodium alginate have been effectively used for the removal of heavy metals (Jamshaid et al., 2019). At the same time, there are many reports in the literature regarding activated carbon functionalized beads for uses in environmental remediation due to their high surface area and functional groups (Nasrullah et al., 2018). Owing to these reasons, the activated carbon is coupled with composite beads. One of the basic issue with adsorbent materials include their separation from treated solution. Thus the solid activated carbon functionalized materials are doped with magnetic nanoparticles, such as nano-zerovalent copper (nZVCu) (Pandi and Viswanathan, 2015). The nano-composite adsorbent can be easily separated from solution by simply applying magnetic field and consequently enhances the reusability of adsorbent material. Additionally, nZVCu was doped to improve stability and loading efficiency of the synthesized activated carbon (AC) functionalized HA and alginate beads. Among the nanomaterials, nZVCu is selected due to its enhance catalytic activity and non-toxic nature (Huang et al., 2012). The new AC and nZVCu coupled HA and alginate beads were investigated for the removal of arsenic As^{3+} from aqueous solutions.

The objectives of this study were to: introduce a new AC coupled nanocomposite beads (i.e., AC/nZVCu/HA-alginate), characterize the synthesized AC and nano-composite beads for morphological characteristics using X-ray diffraction (XRD),

scanning electron microscope (SEM), energy dispersive spectroscopy (EDS), X-ray photoelectron spectroscopy (XPS), transmission electron microscope (TEM), high resolution transmission electron microscope (HR-TEM), Fourier transform infrared (FTIR) spectroscopy, BET surface area analysis, and thermogravimetric analysis (TGA), investigate the As^{3+} adsorption capacity of the newly synthesized AC coupled nanocomposite beads, investigate the reusability and stability of the synthesized AC and nanocomposite beads as well leaching of Cu ion, and evaluate the effects of the concentrations of As^{3+}, adsorbent dose, and pH on the adsorption behavior of AC and nZVCu composite beads. Different adsorption and kinetic models have been investigated to study the details of adsorption process of As^{3+} on the synthesized AC and nanocomposite beads.

2. Materials and Methods

2.1. Materials

All the chemicals used in this study were of high purity and used as received. Sodium arsenite (i.e., $NaAsO_2$, sodium salt of arsenous acid) at a purity of 99% and obtained from Sigma-Aldrich was used as a source of As^{3+}. Other chemicals, i.e., $CuCl_2$, $NaBH_4$, $CaCl_2$, activated carbon, HA, NaOH, and H_2SO_4 were also of high purity and obtained from BDH, Riedel-DeHaen, and Fisher Scientific. The sodium alginate was purchased from a local supplier. All the solutions were prepared in ultra-pure water (Sartorius arium 611DI, Germany, 18.2 MΩ.cm).

2.2. Synthesis of zerovalent copper nanoparticles (nZVCu)

The nZVCu was synthesized using borohydride based chemical reduction method (Huang et al., 2012). The synthesis procedure include dissolving 1.5 g of $CuCl_2$ in 25 mL

mixture of ethanol and water (3 mL ethanol and 22 mL water) and 1.5 g of sodium borohydride ($NaBH_4$) in 40 mL water. Ethanol was added in $CuCl_2$ solution to prevent oxidation of the synthesized nZVCu and to increase stability of nanoparticles (NPs). The $NaBH_4$ solution was added dropwise (1 drop per 2 seconds) into the $CuCl_2$ solution under vigorous stirring. The vacuum filtration technique was used to separate the nanoparticles (NPs) of Cu from the liquid phase. The synthesized NPs were finally dried in an oven at 40 ^oC for five hours. The synthesized nZVCu was finally stored in air tight N_2 sparged glass vials.

2.3. Preparation of AC-nZVCu/HA-alginate composite beads

The nanocomposite beads were synthesized by mixing activated carbon (1.0 g), nZVCu (1.0 g), HA (2.5 g), and sodium alginate (1.5 g) in the order of HA followed by sodium alginate then activated carbon and finally nZVCu in a beaker and stirred for 2 hours at room temperature. Afterwards, the slurry was added dropwise into 300 mL of 3.0 M $CaCl_2$ with a disposable syringe with continuous stirring. The distance between syringe nozzle and surface of $CaCl_2$ solution was about 3.0 cm. The obtained AC/nZVCu/HA-alginate nanocomposite beads were then left overnight in $CaCl_2$ solution with slow stirring followed by washing with distilled water several times and were dried then in an oven at 40 ^oC for 24 h. The prepared beads were spherical in shape with average diameter of 1.8 mm (range 1.62–1.88 mm). The other three types of beads; nZVCu/HA-alginate, AC/HA-alginate, and HA-alginate were prepared using the same above protocol. All the prepared beads were stored in air tight glass vials.

2.4. Batch scale adsorption of As^{3+}

The synthesized AC/nZVCu/HA-alginate, nZVCu/HA-alginate, AC/HA-alginate, and HA-alginate beads (0.5 g/L) were used for the removal of As^{3+} (i.e., 10 mg/L) in aqueous solution at different times from 0 to 120 minutes. The As^{3+} concentration in aqueous solution and that of Cu ions (leached from nZVCu coupled beads) were measured using Atomic Absorption Spectrophotometer (Hitachi Polarized Zeeman AAS, Z-8200, Japan) following the method described by AOAC (1990). The initial (C_i) and final (C_f) concentration of As^{3+} in mg/L, mass of the adsorbent (M_a) in (g), and volume (V_w) of solution in (L) containing As^{3+} were used to calculate the experimental adsorption capacity at equilibrium $q_e(mg/g)$ using Equation 1a while adsorption q_t at time t was calculated using Equation 1b (Imran et al., 2018).

$$q_e = \left(\frac{C_i - C_f}{M_a}\right) \times V_w \tag{1a}$$

$$q_t = \left(\frac{C_i - C_t}{M_a}\right) \times V_w \tag{1b}$$

Where C_t is the residual concentration of As^{3+} in water sample collected at time t. Moreover, to evaluate the effects of pH on As^{3+} removal, point of zero charge was also measured using electrolyte solution (Aliabadi et al. 2018).

2.5. Reusability assessment of the synthesized solid adsorbent

For reusability assessment, the synthesized AC/nZVCu/HA-alginate, nZVCu/HA-alginate, AC/HA-alginate, and HA-alginate beads were regenerated by washing in 0.5 M NaOH solution after each cycle and used for the removal of As^{3+} for seven consecutive cycles. Since alkali are efficient desorbing agents for desorption of As species, thus NaOH was used in the present study (Zhu et al., 2009).

2.6. Equilibrium and kinetic modeling study of As^{3+} adsorption

The experimental adsorption data with AC/nZVCu/HA-alginate, nZVCu/HA-alginate, AC/HA-alginate, and HA-alginate solid adsorbent materials were validated with equilibrium and kinetic adsorption isotherm models. Langmuir (Equation 2−3), Freundlich (Equations 4−5), Temkin (Equation 6), and Dubinin-Radushkevich (Equation 7) models were employed to study equilibrium adsorption data while adsorption kinetics was studied with *pseudo-first-order* (PFO) and *pseudo-second-order* (PSO) kinetic models.

The values of Langmuir model parameters $q_{\max}$ and q_e were calculated from the slope and intercept of linearized form of Equation 3 (Subramani and Thinakaran, 2017).

$$q_e = \frac{K_L C_e q_{\max}}{1 + K_L C_e} \quad \text{(Non-linear form)} \tag{2}$$

$$\frac{C_e}{q_e} = \frac{1}{K_L q_{\max}} + \frac{C_e}{q_{\max}} \quad \text{(Linearized form)} \tag{3}$$

where q_e is adsorption capacity at equilibrium, K_L is Langmuir adsorption constant, C_e is equilibrium concentration, and q_{max} refer to the maximum adsorption at equilibrium. Freundlich model is expressed in Equation (4) and Equation (5) (Saravanan et al. 2018).

$$q_e = K_F C_e^{1/n} \quad \text{(Non-linear form)} \tag{4}$$

$$\ln(q_e) = \left[\ln(K_F) + \left(\frac{1}{n}\right) \ln(C_e) \right] \quad \text{(Linearized form)} \tag{5}$$

Where q_e is the equilibrium sorption, K_F is Freundlich adsorption constant, and $\frac{1}{n}$ is adsorption intensity showing adsorbent heterogeneity. The values of Freundlich model

parameters were calculated from the slope and intercept of the curve between ln(C_e) versus ln(q_e).

In Temkin model (Equation 6), adsorption energy is reduced linearly with coverage of the adsorbent surface.

$$q_e = BK_T + B\ln(C_e) \quad \text{(Linearized form)} \tag{6}$$

Where $B = \frac{RT}{b}$ and K_T are equilibrium adsorption constant and Temkin model constant, respectively. A plot between q_e and $\ln(C_e)$ was used to calculate the values of Temkin model parameters (b and K_T) from the slope and intercept of the curve.

Dubinin-Radushkevich (DR) equilibrium isotherm model (Equation 7) is more general than Langmuir isotherm model as adsorption potential of all the active sites is not uniform (Saravanan et al., 2018).

$$\ln(q_e) = \ln(q_m) - k_{DR}\left(RT \times \ln\left(1+\frac{1}{C_e}\right)^2\right) \quad \text{(Linearized form)} \tag{7}$$

The values of DR model parameters (q_m, k_{DR}) were found from the graph of $\ln(q_e)$ versus $\varepsilon^2 = RT \times \ln\left(1+\frac{1}{C_e}\right)^2$.

The mean free energy of sorption (E) using Dubinin-Radushkevich was computed using Equation (8) (Saravanan et al., 2018; Subramani and Thinakaran, 2017)

$$E = \frac{1}{\sqrt{2k_{DR}}} \tag{8}$$

The kinetic experimental data were analyzed with the linearized form of kinetic

models, *pseudo-first-order* (Equation 9) and *pseudo-second-order* (Equation 10) kinetic models (Imran et al., 2018).

$$log(q_e - q_t) = \left[\log(q_e) - \left(\frac{k_1}{2.303} \right) \times t \right] \quad (9)$$

$$\frac{t}{q_t} = \frac{1}{k_2 (q_e)^2} + \frac{t}{q_e} \quad (10)$$

Where q_e represents simulated adsorption of As^{3+} at equilibrium; q_t is adsorption of As^{3+} at time (t), k_1 is *pseudo-first-order* rate constant and k_2 is *pseudo-second-order* rate constant. In the case of *pseudo-first-order* kinetic model, the values of model parameters were calculated from the slope and intercept of a graph between $log(q_e - q_t)$ versus t. While the values of *pseudo-second-order* kinetic model parameters were calculated from the curve drawn between t versus $\frac{t}{q_e}$.

2.7. Characterization of solid adsorbent materials

The crystalline size of the AC/nZVCu/HA-alginate, nZVCu/HA-alginate, AC/HA-alginate, and HA-alginate solid adsorbents were calculated with XRD (Rigaku Ultima III diffractometer). The XRD data were recorded using a radiation source of CuKα (40 kV, 30 mA) and NaI as a detector.

The surface morphology and elemental composition of the synthesized beads (AC/nZVCu/HA-alginate, nZVCu/HA-alginate, AC/HA-alginate, and HA-alginate) was studied by scanning electron microscopy (SEM) (TESCAN VEGA, LMU) coupled with energy-dispersive X-Ray spectroscopy (EDS) (INCAx-act, Oxford Instruments) operating at 20 kV. Prior to SEM studies, the samples were gold coated with a Balzers' spluttering device.

The X-ray photoelectron spectroscopy (XPS, PHI-5300, ESCA) using Al Kα as an exciting X-ray source and operated at a 50 eV pass energy was used to investigate the surface chemical composition and electronic structure of the synthesized nZVCu.

The analysis of transmission electron microscope (TEM) and high resolution transmission electron microscope (HR-TEM) (FEI-Tecnai TF-20) with field emission gun of 200 kV was done to investigate crystal structure of the nZVCu used in the synthesis of the solid adsorbent materials.

The IR spectra were recorded using Thermo Scientific Nicolet-6700TM FTIR spectrometer in the range from 400 to 4000 cm^{-1} to identify functional groups and bonding environment in the synthesized AC/nZVCu/HA-alginate, nZVCu/HA-alginate, AC/HA-alginate, and HA-alginate beads.

Micromeritics 3Flex (Micromeritics Instrument Corp., Norcross, GA, USA) was used to determine the Brunauer-Emmett–Teller (BET) surface area, Barrett–Joyner–Halenda (BJH) pore size distribution, and pore volume of the synthesized AC/nZVCu/HA-alginate, nZVCu/HA-alginate, AC/HA-alginate, and HA-alginate beads. N_2 adsorption was performed at 77 K. Prior to the measurements, the samples were degassed overnight at 120 ^{o}C.

Thermal analyses of the prepared beads (AC/nZVCu/HA-alginate, nZVCu/HA-alginate, AC/HA-alginate and HA-alginate) were conducted on a Perkin-Elmer thermogravimetric analyzer (STA 6000) with a heating rate of 10 °C·min^{-1} in the temperature range from 30 to 800 °C under nitrogen atmosphere.

3. Results and Discussion

3.1. Characterization of the solid adsorbent materials

The XRD analysis of the synthesized solid adsorbent materials (AC/nZVCu/HA-alginate, nZVCu/HA-alginate, AC/HA-alginate, and HA-alginate beads) was performed, however, only AC/nZVCu/HA-alginate and nZVCu-HA-alginate showed peaks (Figure 1a). The results show both the nanocomposite beads to be highly polycrystalline which could be due to nZVCu. The XRD spectra showed nZVCu peaks at 2θ position of 44^{o} and 52^{o} (JCPDS 89-2838) and small peaks of cuprous oxides at 2θ position of 35^{o} and 65^{o} (JCPDS 05-0667). These finding were consistent with the XRD findings of nZVCu in previous study (Huang et al. 2012). Furthermore, the diffraction peaks of the synthesized AC/nZVCu/HA-alginate beads and nZVCu-HA-alginate beads shows sharp and intense nature which can be attributed to the crystalline nature of the synthesized material due to

nZVCu coupling. The crystallite size (D) of the synthesized materials along the (hkl) profile were calculated from the full width at half maxima of the sharp intense peak applying Scherrer Equation (11a) as given below (Khan et al., 2014).

$$D = \frac{K\lambda}{\beta \cos\theta} \quad (11a)$$

where K is the shape factor equal to 0.89, λ is the wavelength of X-ray of Cu Kα radiation (0.154 nm), β is the full width at half maximum (FWHM) of the peak, and θ is the diffraction angle. The revised Scherrer Equation (11b) was obtained after putting the values of K and λ.

$$D = \frac{0.13706}{\beta \cos\theta} \quad (11b)$$

Putting the values of β and θ, the crystallite size of AC/nZVCu/HA-alginate beads and nZVCu/HA-alginate beads were calculated to be 67 and 59 nm, respectively. This reduction in the crystallite size may be contributed due to the segregation of AC at the solid adsorbent material boundary which inhibits the growth of solid adsorbent materials by restricting direct contact of grains

Figure 1b shows the SEM-EDS analysis of the synthesized HA-alginate, nZVCu/HA-alginate, AC/HA-alginate, and AC/nZVCu/HA-alginate beads. Scanning electron microscopy was performed at 5k magnification. The surfaces of all the synthesized beads were found to be rough and porous. The surface also showed large number of wide voids having different sizes. The rough, porous and wide spaces on the surfaces are attributed to the molecular diffusions (Nasrullah et al., 2018). Thus, the prepared porous beads will facilitate maximum removal of As^{3+} from aqueous solution. The surface properties of the prepared beads are similar as reported by Hassan et al., (2014) for alginate-based beads.

The surface morphologies of the beads containing activated carbon (AC/HA-Alginate and AC/nZVCu/HA-Alginate) were similar as shown in Figure 1b (C−D) while in HA-Alginate beads there are round structures along with a rough surface (Figure 1b (A)). The Cu containing beads (nZVCu/HA-Alginate) shows micro structures of Cu on its surface (Figure 1b (B and D)). The energy dispersive X-ray spectroscopy (EDS) analysis shows carbon, oxygen, chloride, calcium and phosphorous elements in the prepared beads (Figure 1b (E−H)). The EDS analysis also confirms the presence of copper element in the Cu containing beads (i.e., nZVCu/HA-Alginate and AC/nZVCu/HA-Alginate beads) (Figure 1b (G and H)).

The XPS measurements were made to analyze the surface chemical composition. The narrow Cu 2p is shown in Figure 1c (A). It can be seen that the main characteristic peaks for Cu^0 (nZVCu) at binding energies of $2p_{3/2}$ and $2p_{1/2}$ were at 932.8 eV and 952.8 eV, respectively (Dong et al., 2014). Thus, it confirms the successful synthesis of nZVCu. Furthermore, a shake-up satellite peaks at 945.45 and 962.27 eV could be attributed to the open $3d^9$ shell of Cu^{2+} ions (Anandan et al., 2012).

In addition, Figure 1c (B) depicts the high resolution spectra of O1s. The peaks located at 532.8 eV, 531.4 eV, and 529.9 eV, respectively, are assigned to oxygen in the outermost layer of adsorbed H_2O, oxygen atoms in the surface hydroxyl groups (O–H), and oxygen in the lattice (M–O) (Peng et al., 2016). Figure 1d (A) display the low magnification transmission electron microscopy (TEM) image of nZVCu. It can be seen that the nZVCu particles are smaller in size ranging from 50 to100 nm and are homogenously distributed with less aggregation. Moreover, Figure 1d (B) indicates that the synthesized nZVCu particles have good crystallinity and are formed at nano-scale.

Figure 1e illustrates the FTIR spectra of the prepared AC/nZvCu/HA-alginate, nZvCu/HA-alginate, AC/HA-alginate, and HA-alginate beads. The vibrational bands between 3200 and 3500 cm^{-1}, assigned to O–H groups and N–H stretching were observed for hydroxyapatite, alginates, and activated carbon in the composite beads (Muhammad et al., 2016; Shu et al., 2017). The peak around 1600-1610 cm^{-1} was due to C-O and C–C vibrations in alginate and activated carbon, respectively (Yakout et al., 2016). The symmetric stretching vibrations were observed between 1420−1440 cm^{-1}, corresponding to carboxylate salt (Iqbal et al., 2018). Albeit, the peak was shifted from 1440 to 1420 cm^{-1} with the addition of activated carbon. This might be a result of pi-pi interaction between aromaticity of activated carbon and unsaturated carbonyl group of carboxylate salt. The peak observed at 1010−1040 cm^{-1} was attributed to the asymmetric stretching of phosphate group (PO_4^{3-}) of hydroxyapatite, and carboxylate and ether structure of activated carbon in the composite beads (Muhammad et al., 2016).

The N_2-adsorption-desorption isotherms were used to determine the BET surface area of the synthesized AC/nZVCu/HA-alginate, nZVCu/HA-alginate, AC/HA-alginate, and HA-alginate beads (Figure 1f). The surface analysis indicated BET surface area to be 45.1, 29.3, 25.7, and 11.4 m^2/g for AC/nZVCu/HA-alginate, nZVCu/HA-alginate, AC/HA-alginate, and HA-alginate beads, respectively. The N_2-adsorption-desorption isotherms gave average pore size of 4.5, 3.6, 3.1, and 2.4nm and pore volume of 0.0443, 0.0305, 0.0278, and 0.016 cm^3/g for the prepared AC/nZVCu/HA-alginate, nZVCu/HA-alginate, AC/HA-alginate, and HA-alginate beads, respectively. The high surface area of suggest the mesoporous nature of the synthesized solid adsorbent materials. Further, it was found that coupling AC and nZVCu increased the surface area, pore size, and pore

volume of the prepared HA-alginate beads. The hysteresis loop observed in N_2 adsorption-desorption are due to capillary condescension on the mesoporous surface.

Thermogravimetric analysis (TGA) was performed under nitrogen atmosphere for the prepared AC/nZVCu/HA-alginate, nZVCu/HA-alginate, AC/HA-alginate, and HA-alginate beads in the temperature range from 30 ^{o}C to 800 ^{o}C with heating rate of 10 ^{o}C/min (Figure 1g). The weight loss below 120 ^{o}C was assigned to moisture attached to the surface of beads. The results demonstrated nZVCu/HA-alginate beads to be more stable with no significant decomposition until 300 ^{o}C. However, the AC/nZVCu/HA-alginate beads were slightly less stable and 17 wt% was lost at around 300 ^{o}C. This means that mixing of AC caused a slight decrease in thermal stability of the beads. Nasrullah et al., (2018) observed that mixing of AC with alginate resulted in decreasing the thermal stability of the beads. AC contain chemical groups, such as COOH that act as a bronsted acid and contributes in the decomposition of the polymeric matrix (Nasrullah et al., 2018). The AC/HA-alginate beads exhibited the highest weight loss (27%) at 300 ^{o}C. The weight loss in the region 200-400 ^{o}C was due to the conversion of HPO_4^{2-} to pyrophosphate ($P_2O_7^{4-}$) in HA (Manatunga et al., 2018). The weight loss after 400 ^{o}C was due to the decomposition of the alginate polymer.

3.2. Performance of the beads in the removal of As^{3+}

The performance of prepared four types of nanocomposite beads was investigated for the removal of As^{3+} (i.e., 10 mg/L) from aqueous solutions with different treatment times i.e., 0 to 120 min. The results are shown in Figure 2 which depicts that removal of As^{3+} was 95, 56, 52, and 39% by AC/nZVCu/HA-alginate, nZVCu/HA-alginate, Ac/HA-alginate, and HA-alginate solid adsorbent materials, respectively, after 120 min. These

results can be explained on the basis of BET surface area results which indicated that the highest surface area was observed for AC/nZVCu/HA-alginate and least one was for HA-alginate and consequently achieved maximum removal of As^{3+} in the former in our study. These results further suggest that modifying HA-alginate beads with AC and zerovalent copper led to the enhanced performance of the beads and was in agreement with the previous study (Benhouria et al., 2015). The removal efficiency of As^{3+} by the synthesized beads was fast in the start of treatment and slower at later stages. The possible reason for this trend could be the saturation of active sites and lowering in initial concentration of As^{3+} at the later treatment stages and vice versa and was consistent to the trend observed in a previous study (Nasrullah et al., 2018).

The adsorption of metal ions on the surface of solid adsorbent materials is governed by the number of active sites as well as the functional groups for complexation reaction. The synthesized HA-alginate beads several functional groups, such as COOH that might play role in the adsorption of As^{3+}. The coupling of nZVCu and AC provide the source of more functional groups and metal ions for complexation and exchange reactions of As^{3+}.

3.3. Reusability assessment of the solid adsorbent materials

The reusability assessment of the prepared solid adsorbent materials is highly essential for potential practical applications. In the present study, reusability of the prepared AC/nZVCu/HA-alginate, nZVCu/HA-alginate, AC/HA-alginate, and HA-alginate beads was investigated for seven consecutive cycles. The results as shown in Figure 3 revealed that the removal of As^{3+} by the AC/nZVCu/HA-alginate, nZVCu/HA-alginate, AC/HA-alginate, and HA-alginate beads was 99%, 71%, 65%, and 53%, respectively in the first run. At fourth run of adsorption, the removal of As^{3+} was found to

be 95%, 64%, 53%, and 25% by AC/nZVCu/HA-alginate, nZVCu/HA-alginate, AC/HA-alginate, and HA-alginate beads, respectively (Figure 3). The removal of As^{3+} was finally investigated at seventh run of treatment and found to be 88%, 50%, 40%, and 8% by AC/nZVCu/HA-alginate, nZVCu/HA-alginate, AC/HA-alginate, and HA-alginate beads, respectively (Figure 3). The results indicate that modifying HA-alginate beads with both AC and nZVCu showed greater reusability and can be used repeatedly without considerable loss in adsorption efficiency.

3.4. Cu ion leaching from nZVCu loaded solid adsorbent materials

The Cu ion leached from nZVCu coupled nanocomposite beads was investigated using atomic absorption spectroscopy method as described above and found to be 0.03 mg/L. The analyzed concentration of Cu ion was much below than the United State Environmental Protection Agency (USEPA) maximum allowable concentration of Cu ion (i.e., 1.3 mg/L) in water.

3.5. Effects of initial concentrations of As^{3+}

The study of the effects of initial concentration of contaminants is beneficial for potential applications of the adsorbent. The saturation of the adsorbent surface is driven by the initial concentration of the contaminant. In the present study, the removal efficiency of As^{3+} was studied under different concentrations from 5 to 20 mg/L at a constant dose of adsorbent material (i.e., 0.5 g/L). Figure 4 depicts an increase in the removal efficiency of As^{3+} by the synthesized composite beads with increasing initial concentrations of As^{3+} and was in agreement with a previous study (Nasrullah et al., 2018). At initial stage, there was rapid increase in As^{3+} adsorption with increase in As^{3+} concentration because there was higher diffusion of the contaminant. The observed result

could be due to the maximum availability of As^{3+} for adsorption on the surface of adsorbent at high As^{3+} concentrations than at lower As^{3+} concentration (Nasrullah et al., 2018). Another possible reason could be the mass transfer driving force that enables interactions between adsorbent and adsorbate, which has been reported to be high at high concentration of adsorbate (Nasrullah et al., 2018).

3.6. Effects of pH

The effects of pH on the adsorption process are important to be investigated for the potential practical applications of AC and nZVCu coupled beads since pH of wastewater can vary between acidic and basic waters. Besides, pH can significantly affect the charge on the surface of adsorbent, the activity of functional groups present on the surface of adsorbent and also the speciation of metal ions (Azouaou et al., 2010; Wei et al., 2015). The aqueous chemistry and binding sites on the surface of the adsorbent are also affected by pH. The measurement of point of zero charge (PZC) is important to know the nature of the adsorbent under different pH (Sigdel et al., 2016). The PZC measured for HA-alginate, AC/HA-alginate, nZVCu/HA-alginate and AC/nZVCu/HA-alginate adsorbent materials was 7.61, 8.25, 9.1 and 8.85, respectively. Removal of As^{3+} by the synthesized AC/nZVCu/HA-alginate beads was thus investigated under different pH conditions from 3 to 10.5. The results are presented in Figure 5 which shows a maximum removal of As^{3+} at pH 5.8 and minimum at pH 10.5 and pH 3.0. A possible reason could be the increased electrostatic interaction between As^{3+} and the adsorbent at pH 5.8. Arsenic is adsorbed as arsenite or arsenate and in our scenario As^{3+} was adsorbed as arsenite (As^{3+}) and its maximum removal was favored at pH < PZC. At pH < PZC, solution is rich in H^+ ions and favors the adsorption of As^{3+}.The PZC of the adsorbents used in the present study

was more than 7.6. Similar trend has been observed in previous study (Sigdel et al., 2016). It has been reported that zerovalent metals donates electron to aqueous solution that reduces proton to hydrogen gas in the solution and, consequently, led to great electrostatic interaction between the adsorbent and adsorbate (Badruddoza et al., 2011). The lower removal efficiency of As^{3+} by AC/nZVCu/HA-alginate beads under pH < 5.0 and pH > 7.0 could be due to greater mobility of H_3O^+ in the aqueous solution that consequently compete with As^{3+} for active sites as well as precipitation of metal (Badruddoza et al., 2011).

3.7. Effects of adsorbent dosage

Surface area and number of active sites available for the adsorption are governed by the dose of the adsorbent material (Kumar and Kumaran, 2005). The effects of adsorbent doses ranging from 0.5 to 2.0 g/L were evaluated on the removal of As^{3+} at an initial concentration of 10 mg/L. The results are shown in Figure 6 which depicts that the increase in adsorbent material dosage correspondingly increased the removal efficiency of As^{3+}. It has been reported that increasing dosage of adsorbent consequently led to availability of more active sites for adsorption of the contaminants and provided sufficient support to our findings (Kumar and Kumaran, 2005).

3.8. Equilibrium and kinetic adsorption modeling

The experimental results obtained at equilibrium under isothermal conditions were tested using Langmuir, Freundlich, Temkin and DR models as already explained in the methodology section. The models' parameters (Table 1) were calculated from the slope and intercept of the curves and are given in Figure 7 (a−d) for each model. The values of models' parameters varied depending on the characteristics of the adsorbent materials.

The suitability of the model was assessed with the value of regression coefficient (R^2). Our experimental results were best fitted with Freundlich model (R^2 = 0.97-0.998) with all types of beads followed by Temkin (R^2 = 0.95-0.998), Langmuir model (R^2 = 0.94-0.99) and DR model (R^2 = 0.83-0.958). In case of Freundlich model, it is reported that if the value of $n > 1$, the adsorbent material gives non-linear physical adsorption (Saravanan et al., 2018). Our results showed $n > 1$ with all the adsorbents and the involved adsorption is physical. The maximum value of *n* calculated was 2.59. The value of E (Table 1) also suggests that the adsorption involved with the HA-alginate beads and their composites with nZVCu and AC is physical. The adsorption isotherm using C_e vs q_e was also plotted for all the solid adsorbent materials as shown in Figure 7e.

The kinetics of experimental data were fitted with *pseudo-first-order* and *pseudo-second-order* kinetic models. The experiments for kinetics evaluation with all the four adsorbents (AC/nZVCu/HA-alginate, nZVCu/HA-alginate, AC/HA-alginate, and HA-alginate beads) were carried out at As^{3+} concentration (10 mg/L) and samples were collected after 5, 10, 20, 40, 80 and 120 min at 0.5 g/L dosage of each adsorbent separately. The values of the kinetic model parameters are also given in Table 1 and were calculated from the slope and intercept of the curves given in Figure 8 (a and b) for each adsorbent. Our experiments were well explained with *pseudo-second-order* kinetic model as compared with *pseudo-first-order* model based on the value of R^2 which was > 0.99 for AC/nZVCu/HA-alginate, nZVCu/HA-alginate, AC/HA-alginate, and HA-alginate beads. In Figure 8 (c and d), experimental q_t has been plotted vs calculated q_t obtained from *pseudo-first-order* and *pseudo-second-order* which also shows that *pseudo-second-order* best described our experimental results.

Based on comparison of adsorption and kinetic parameters of this solid adsorbent material with other adsorbent in the same field in previous studies (Sigdel et al., 2016) suggested our material to be of greater interest.

4. Conclusion

In this study, AC and nZVCu coupled beads were successfully prepared and effectively used for the removal of As^{3+} from aqueous solutions. The AC and nZVCu composites with HA-alginate beads showed high performance in the removal of As^{3+} (i.e., 39.06 mg/g) compared to 13.96 mg/g by HA-alginate beads only. The nZVCu composite beads were found to be very stable at high temperature. The coupling of AC and nZVCu was found to increase the surface area, pore size, and pore volume as well as reusability of the prepared HA-alginate beads and thus led to the maximum removal of As^{3+} as compared to HA-alginate beads even after seven cyclic runs. An increase in the concentration of As^{3+} and dosage of adsorbent promoted the adsorption of As^{3+}. The removal of As^{3+} by the prepared beads was studied by different adsorption and kinetic models where Freundlich adsorption and *pseudo-second-order* kinetic models were found to be well-fitted. On the whole, the developed composite beads showed the potential to be applied as adsorbent in different water treatment applications for the removal of As^{3+}.

Acknowledgment

The research was supported by the research cluster grant (R18029) from Zayed University, Abu Dhabi, United Arab Emirates and COMSATS University Research Grant Program (CRGP).

References

Ahmed, E.S., Moustafa, H.Y., El-Masry, A.M., Hassan, S.A., 2014. Natural and synthetic polymers for water treatment against dissolved pharmaceuticals. J. Apply. Polym. Sci. 131, 40458−40468.

Aliabadi, H.M., Saberikhah, E., Pirbazari, A.E., Khakpour, R., Alipour, H., 2018. Triethoxysilylpropylamine modified alkali treated wheat straw: an efficient adsorbent for methyl orange adsorption. Cellulose Chem Technol. 52, 129–140.

Amini, M., Abbaspour, K.C., Berg, M., Winkel, L., Hug, S.J., Hoehn, E., Yang, H., Johnson, C.A., 2008. Statistical modeling of global geogenic arsenic contamination in groundwater. Environ. Sci. Technol. 42, 3669−3675.

Anandan, S., Lee, G.J. Wu, J.J., 2012. Sonochemical synthesis of CuO nanostructures with different morphology. Ultrason. Sonochem. 19, 682−686.

Azouaou, N., Sadaoui, Z., Djaafri, A., Mokaddem, H., 2010. Adsorption of cadmium from aqueous solution onto untreated coffee grounds: Equilibrium, kinetics and thermodynamics. J. Hazard. Mater. 184,126−34.

Badruddoza, A.Z.M., Tay, A.S.H., Tan, P.Y., Hidajat, K., Uddin, M.S., 2011. Carboxymethyl-bcyclodextrin conjugated magnetic nanoparticles as nano-adsorbents for removal of copper ions: Synthesis and adsorption studies. J. Hazard. Mater. 185, 1177–1186.

Benhouria, A., Azharul Islam, Md., Zaghouane-Boudiaf, H., Boutahala, M., Hameed, B.H., 2015. Calcium alginate–bentonite–activated carbon composite beads as highly effective adsorbent for methylene blue. Chem. Eng. J. 270, 621−630.

Chemists, A.O.A., Cunniff, P. 1990. Official methods of analysis Association of Official Analytical Chemists. (Inc). AOAC Inc. Arlington, VA, USA.

Dong, G., Ai, Z., Zhang, L., 2014. Total aerobic destruction of azo contaminants with nanoscale zero-valent copper at neutral pH: Promotion effect of in-situ generated carbon center radicals. Water Res. 66, 22−30.

Hamayun, M., Mahmood, T., Naeem, A., Muska, M., Din, S.U., Waseem, M., 2014. Equilibrium and kinetics studies of arsenate adsorption by $FePO_4$. Chemosphere 99, 207−215.

Hassan, A.F., Abdel-Mohsen, A.M., Fouda, M.M.G., 2014. Comparative study of calcium alginate, activated carbon, and their composite beads on methylene blue adsorption. Carbohydr. Polym. 102, 192−198.

Huang, C.-C., Lo, S.-L., Lien, H.-L., 2012. Zero-valent copper nanoparticles for effective dechlorination of dichloromethane using sodium borohydride as a reductant. Chem. Eng. J. 203, 95−100.

Imran, M., Suddique, M., Shah, G., Ahmad, I., Murtaza, B., Shah, N., Mubeen, M., Ahmad, S., Zakir, A., Schotting, R., 2018. Kinetic and equilibrium studies for cadmium biosorption from contaminated water using Cassia fistula biomass. International. J. Environ. Sci. Technol. 1-10.

Iqbal, B., Sarfaraz, Z., Muhammad, N., Ahmad, P., Iqbal, J., Khan, Z.U.H., Gonfa, G., Iqbal, F., Jamal, A., Rahim, A., 2018. Ionic liquid as a potential solvent for preparation of collagen-alginate-hydroxyapatite beads as bone filler. J. Biomater. Sci. Polym. Ed. 29, 1168−1184.

Jamshaid, A., Iqbal, J., Hamid, A., Ghauri, M., Muhammad, N., Nasrullah, A., Rafiq, S.,

Shah, N.S., 2019. Fabrication and Evaluation of Cellulose-Alginate-Hydroxyapatite Beads for the Removal of Heavy Metal Ions from Aqueous Solutions. Z. Phys. Chem. DOI: 10.1515/zpch-2018−1287.

Khan, J.A., Han, C., Shah, N.S., Khan, H.M., Nadagouda, M.N., Likodimos, V., Falaras, P., O'Shea, K., Dionysiou, D.D., 2014. Ultraviolet–visible light–sensitive high surface area phosphorous-fluorine–co-doped TiO_2 nanoparticles for the degradation of atrazine in water. Environ. Eng. Sci. 31, 435–446.

Kumar, K.V., Kumaran, A., 2005. Removal of methylene blue by mango seedkernel powder. Biochem. Eng. J. 27, 83–93.

Lesmana, S.O., Febriana, N., Soetaredjo, F.E., Sunarso, J., Ismadji, S., 2009. Studies on potential applications of biomass for the separation of heavy metals from water and wastewater. Biochem. Eng. J. 44,19−41.

Li, L., Iqbal, J., Zhu, Y., Zhang, P., Chen, W., Bhatnagar, A., Du, Y., 2018, Chitosan/Ag-hydroxyapatite nanocomposite beads as a potential adsorbent for the efficient removal of toxic aquatic pollutants. Int. J. Biol. Macromol. 120, 1752−1759.

Manatunga, D.C., de Silva, R.M., Nalin de Silva, K.M., de Silva, N., Premalal, E., 2018. Metal and polymer-mediated synthesis of porous crystalline Hydroxyapatite nanocomposites for environmental remediation. R. Soc. Open Sci. 5, 171557.

Martinez, V.D., Vucic, E.A., Becker-Santos, D.D., Gil, L., Lam, W.L., 2011. Arsenic exposure and the induction of human cancers. J. Toxicol. 2011, 431287.

Mohan, D., Pittman, C.U., 2007. Arsenic removal from water/wastewater using adsorbents-A critical review. J. Hazard Mater. 142, 1−53.

Muhammad, N., Gao Y., Iqbal, F., Ahmad, P., Ge, R., Nishan, U., Rahim, A., Gonfa, G.,

Ullah, Z., 2016. Extraction of biocompatible hydroxyapatite from fish scales using novel approach of ionic liquid pretreatment. Sep. Purif. Technol. 161, 129−135.

Murtaza, B., Shah, N.S., Sayed, M., Khan, J.A., Imran, M., Shahid, M., Khan, Z.U.H., Ghani, A., Murtaza, G., Nawshad, M., Khalid, M.S., Niazi, N.K., 2019. Synergistic effects of bismuth coupling on the reactivity and reusability of zerovalent iron nanoparticles for the removal of cadmium from aqueous solution. Sci. Total Environ. 669, 333−341.

Nasrullah, A., Bhat, A.H., Naeem, A., Isa, M.H., Danish, M., 2018. High surface area mesoporous activated carbon-alginate beads for efficient removal of methylene blue. Int. J. Biol. Macromol. 107, 1792-1799.

Nguyen, T.A., Ngo, H.H., Guo, W.S., Zhang, J., Liang, S., Yue, Q.Y., Li, Q., Nguyen, T.V., 2013. Applicability of agricultural waste and by-products for adsorptive removal of heavy metals from wastewater. Bioresour. Technol.148, 574−85.

Pandi, K., Viswanathan, N., 2015. Enhanced defluoridation and facile separation of magnetic nano-hydroxyapatite/alginate composite. Int. J. Biol. Macromol. 80, 341−349.

Peng, B., Song, T., Wang, T., Chai, L., Yang, W., Li, X., Li, C., Wang, H., 2016. Facile synthesis of Fe_3O_4@$Cu(OH)_2$ composites and their arsenic adsorption application. Chem. Eng. J. 299, 15−22.

Saravanan, A., Kumar, P.S., Renita, A.A., 2018. Hybrid synthesis of novel material through acid modification followed ultrasonication to improve adsorption capacity for zinc removal. J. Clean. Prod. 172, 92−105.

Sayed, M., Gul, M., Shah, N.S., Khan, J.A., Khan, Z.U.H., Rehman, F., Khan, A.R., Rauf, R., Arandiyan, H., Yang, C.P., 2019. In-situ dual applications of ionic liquid coated Co^{2+} and Fe^{3+} co-doped TiO_2: Superior photocatalytic degradation of ofloxacin at pilot scale level and enhanced peroxidase like activity for calorimetric biosensing. J. Mol. Liq. 282, 275−285.

Shah, N.S., Khan, J.A., Sayed, M., Khan, Z.U.H., Ali, H.S., Murtaza, B., Khan, H.M., Imran, M. and Muhammad, N., 2019. Hydroxyl and sulfate radical mediated degradation of ciprofloxacin using nano zerovalent manganese catalyzed $S_2O_8^{2-}$. Chem. Eng. J. 356, 199−209.

Shu, J., Song, C., Xia, H., Zhang, L., Peng, J., Li, C., Shang, S., 2017. Copper loaded on activated carbon as an efficient adsorbent for removal of methylene blue. R. Soc. Chem. Adv. **7**, 14395−14405.

Sigdel, A., Park, J., Kwak, H., Park, P.-K., 2016. Arsenic removal from aqueous solutions by adsorption onto hydrous iron oxide-impregnated alginate beads. J. Ind. Eng. Chem. 35, 277–286

Subramani, S., Thinakaran, N., 2017. Isotherm, kinetic and thermodynamic studies on the adsorption behaviour of textile dyes onto chitosan. Process Saf. Environ. Prot. 106, 1−10.

Wei, W., Kim, S., Song, M.-H., Bediako, J.K., Yun, Y.-S., 2015. Carboxymethyl cellulose fiber as a fast binding and biodegradable adsorbent of heavy metals. J. Taiwan Inst. Chem. E. 57,104−10.

WHO, 2011a. Arsenic in Drinking-Water. Background Document for Development of WHO Guidelines for Drinking-water Quality.

http://www.who.int/water_sanitation_health/dwq/chemicals/arsenic.pdf (Accessed 10 November 2017).

WHO, 2011b. Guidelines for Drinking-water Quality, fourth ed. World Health Organization, Geneva http://www.who.int/water_sanitation_health/publications/2011/dwq_guidelines/en (Accessed 10 November 2018).

Yakout, S.M., El-Deen, G.S., 2016. Characterization of activated carbon prepared by phosphoric acid activation of olive stones. Arab. J. Chem. 9, S1155-S1162.

Zhu, H., Jia, Y., Wu, X., Wang, H., 2009. Removal of arsenic from water by supported nano zero-valent iron on activated carbon. J. Hazard. Mater. 172, 1591–1596

Figure Captions

Figure 1a. XRD Spectra of the synthesized AC/nZVCu/HA-alginate and nZVCu/HA-alginate beads.

Figure 1b. SEM images of the synthesized HA-alginate beads (A), nZVCu/HA-alginate beads (B), AC/HA-alginate beads (C), and AC/nZVCu/HA-alginate beads (D).

Figure 1b. EDS spectra of the synthesized HA-alginate beads (E), AC/HA-alginate beads (F), nZVCu/HA-alginate beads (G), and AC/nZVCu/HA-alginate beads (H).

Figure 1c. XPS spectra of Cu 2p (A) and O 1s (B).

Figure 1d. TEM image (A) and HR-TEM image (B) of nZVCu.

Figure 1e. FTIR spectra of the synthesized HA-alginate beads (A), nZVCu/HA-alginate beads (B), AC/HA-alginate beads (C), and AC/nZVCu/HA-alginate beads (D).Figure 1f N_2 adsorption-desorption isotherms of the synthesized beads.Figure 1g. TGA graph of the synthesized beads.

Figure 2. Removal of As^{3+} by HA-alginate, AC/HA-alginate, nZVCu/HA-alginate, and AC/nZVCu/HA-alginate beads. Experimental conditions: $[\text{HA-alginate}]_0$ = $[\text{AC/HA-alginate}]_0$ = $[\text{nZVCu/HA-alginate}]_0$ = $[\text{AC/nZVCu/HA-alginate}]_0$ = 0.5 g/L, $[As^{3+}]_0$ = 10 mg/L, pH = 5.8.

Figure 3. Reusability assessment of the synthesized HA-alginate, AC/HA-alginate, nZVCu/HA-alginate, and AC/nZVCu/HA-alginate beads for removal of As^{3+}. Experimental conditions: $[\text{HA-alginate}]_0$ = $[\text{AC/HA-alginate}]_0$ = $[\text{nZVCu/HA-alginate}]_0$ = $[\text{AC/nZVCu/HA-alginate}]_0$ = 1.0 g/L, $[As^{3+}]_0$ = 10 mg/L, pH = 5.8.

Figure 4. Removal of As^{3+} by AC/nZVCu/HA-alginate beads using different concentrations of As^{3+}. Experimental conditions: $[AC/nZVCu/HA\text{-}alginate]_0$ = 0.5 g/L, $[As^{3+}]_0$ = 5−20 mg/L, pH = 5.8.

Figure 5. Removal of As^{3+} by AC/nZVCu/HA-alginate beads under different pH. Experimental conditions: $[AC/nZVCu/HA\text{-}alginate]_0$ = 0.5 g/L, $[As^{3+}]_0$ = 10 mg/L, pH = 3−10.5.

Figure 6. Removal of As^{3+} by AC/nZVCu/HA-alginate beads under different doses of solid adsorbent materials. Experimental conditions: $[AC/nZVCu/HA\text{-}alginate]_0$ = 0.5−2.0 g/L, $[As^{3+}]_0$ = 10 mg/L, pH = 5.8.

Figure 7. Validation of the removal of As^{3+} by HA-alginate, AC/HA-alginate, nZVCu/HA-alginate, and AC/nZVCu/HA-alginate beads under different equilibrium models: Langmuir model (a), Freundlich model (b), Temkin model (c), and Dubinin Radushkevich (d), and plot of experimental C_e vs q_e (e). Experimental conditions: $[HA\text{-}alginate]_0$ = $[AC/HA\text{-}alginate]_0$ = $[nZVCu/HA\text{-}alginate]_0$ = $[AC/nZVCu/HA\text{-}alginate]_0$ = 0.5 g/L, $[As^{3+}]_0$ = 10 mg/L, pH = 5.8.

Figure 8. Validation of the removal of As^{3+} by HA-alginate, AC/HA-alginate, nZVCu/HA-alginate, and AC/nZVCu/HA-alginate beads under different kinetic models: *Pseudo-first-order kinetic* (a), *Pseudo-second-order* kinetic (b), and comparison of

experimental q_t and q_t calculated from *Pseudo-first-order* and *Pseudo-second-order* kinetic models (c, d). Experimental conditions: $[HA\text{-alginate}]_0$ = $[AC/HA\text{-alginate}]_0$ = $[nZVCu/HA\text{-alginate}]_0$ = $[AC/nZVCu/HA\text{-alginate}]_0$ = 0.5 g/L, $[As^{3+}]_0$ = 10 mg/L, pH = 5.8.

Table Captions

Table 1. Parameters of adsorption isotherm models (Langmuir, Freundlich, Temkin, and Dubinin-Radushkevich) and kinetic models (*pseudo-first-order* and *pseudo-second-order*) applied for the adsorption of As^{3+} (10 mg/L) on 0.5 g/L of HA-alginate, AC/HA-alginate, nZVCu/HA-alginate, and AC/nZVCu/HA-alginate beads at pH 5.8.

Note: The kinetic models were calculated at a reaction time of 10 minutes.

Figure 1a

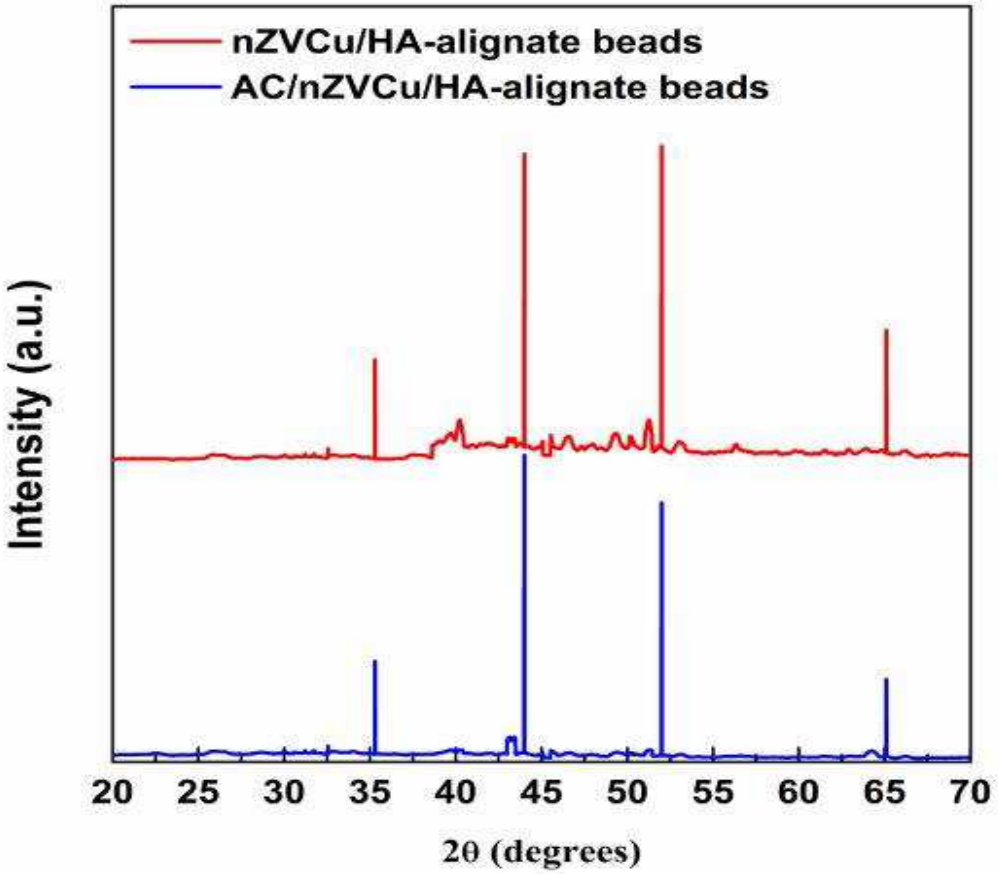
nZVCu/HA-alignate beads
AC/nZVCu/HA-alignate beads
Intensity (a.u.)
20
25
30
35
40
45
50
55
60
65
70
2θ (degrees)

Figure 1b

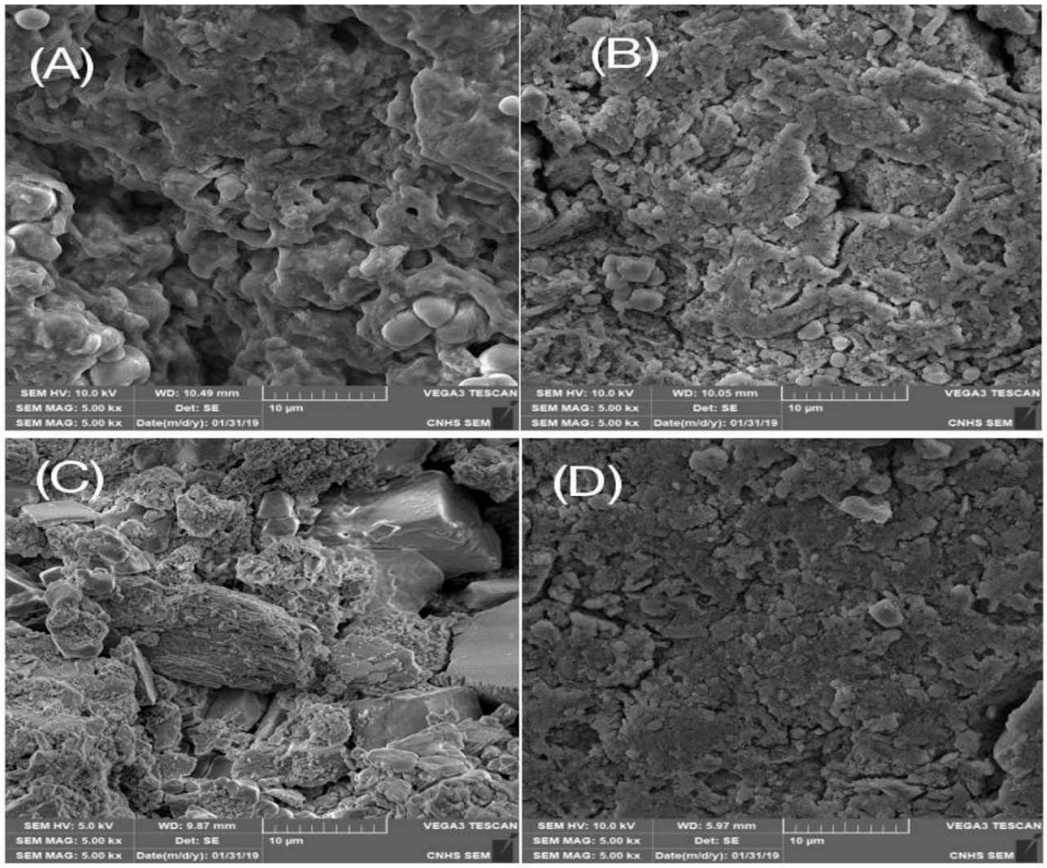

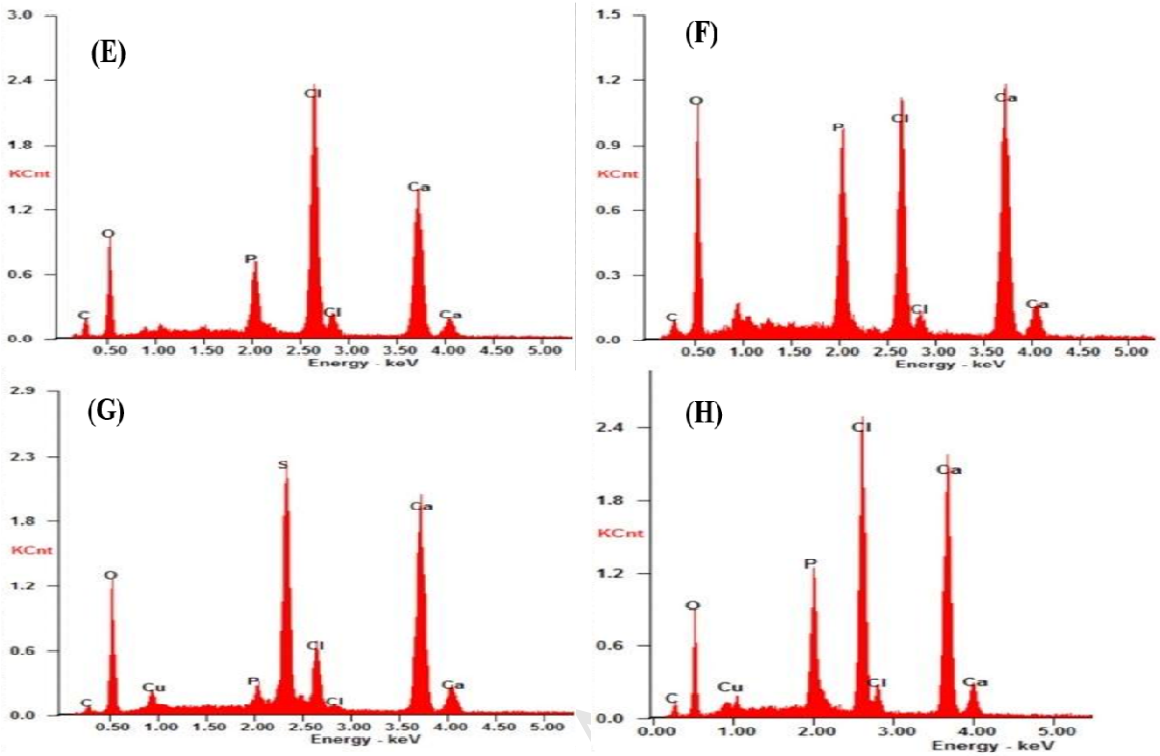

Figure 1c

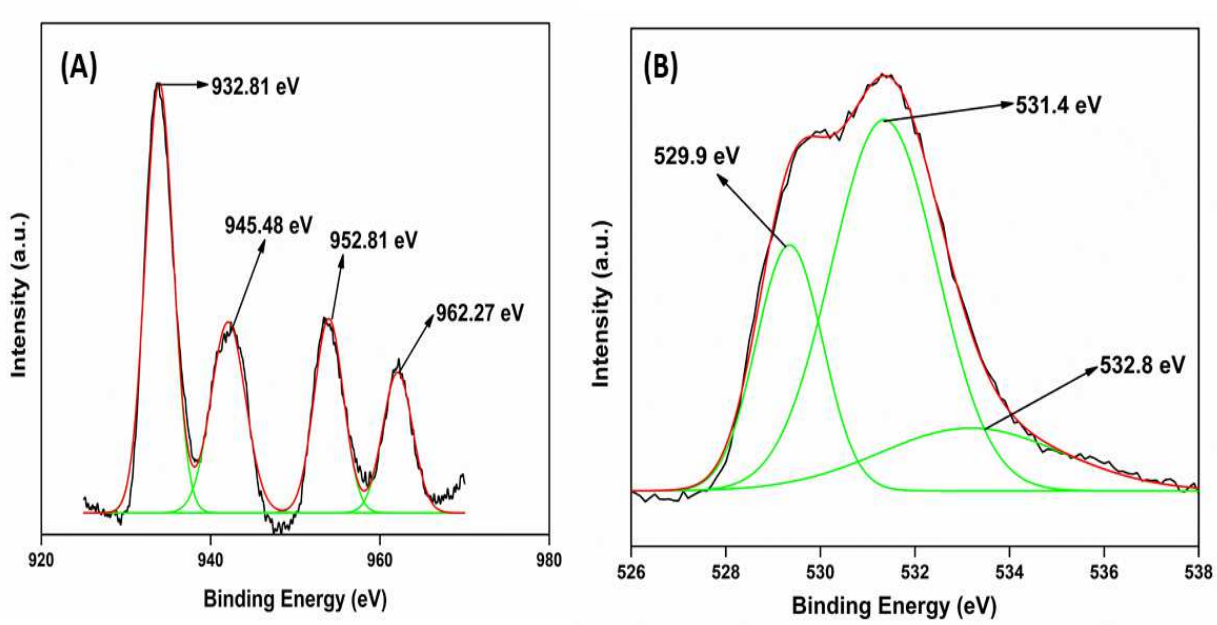

Figure 1d

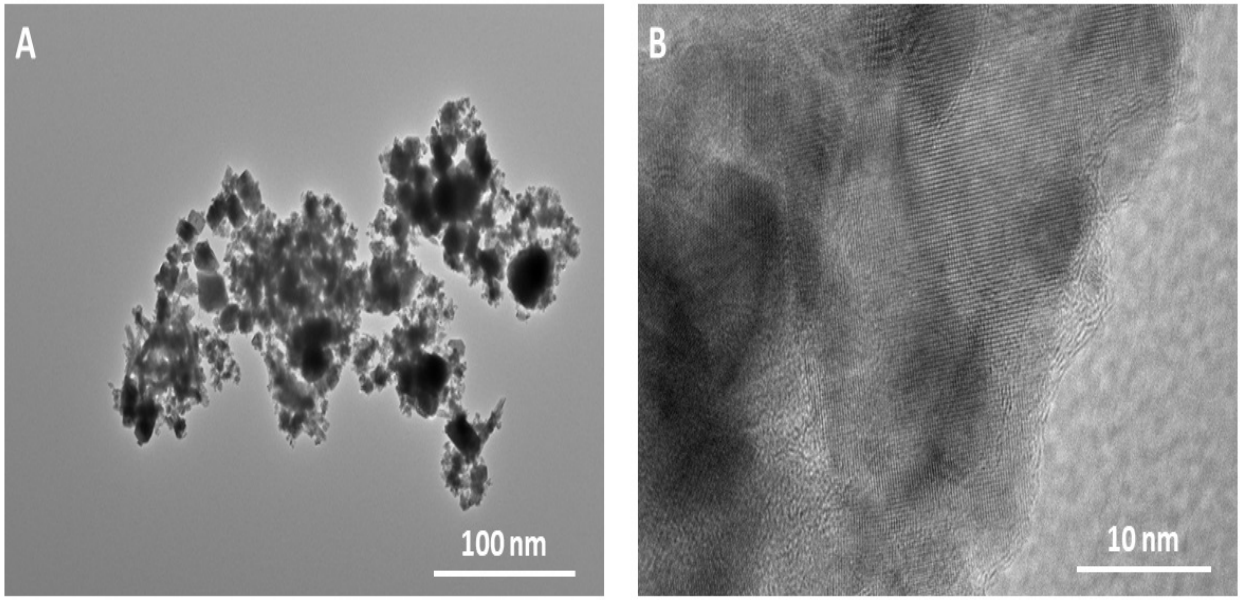

Figure 1e

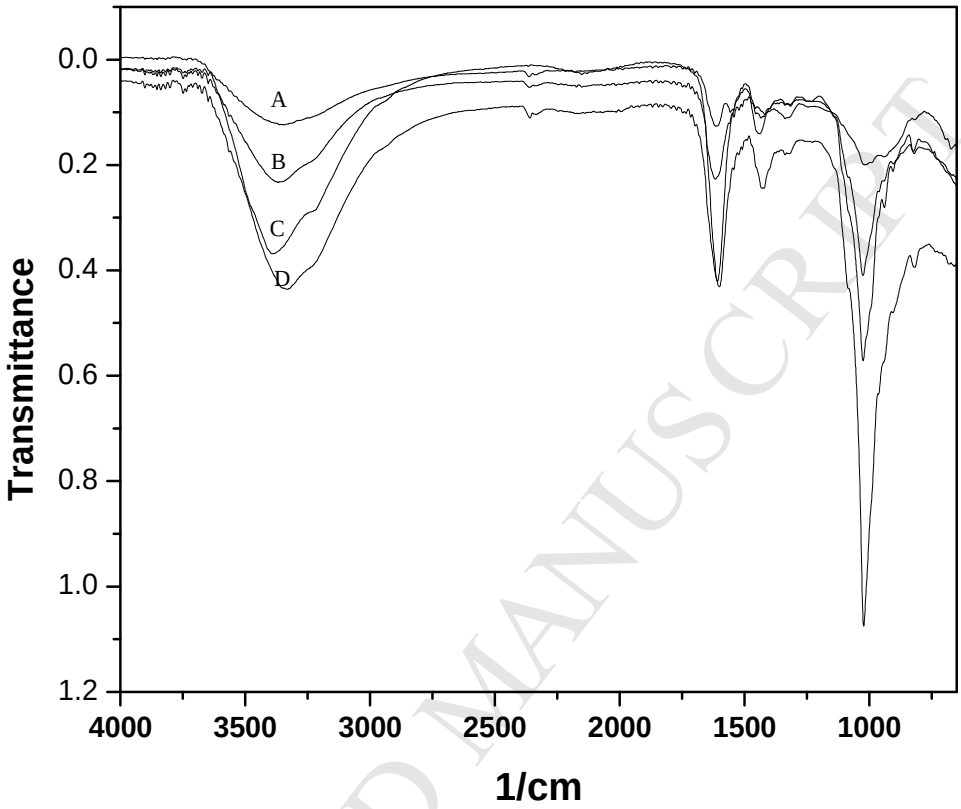

Figure 1f

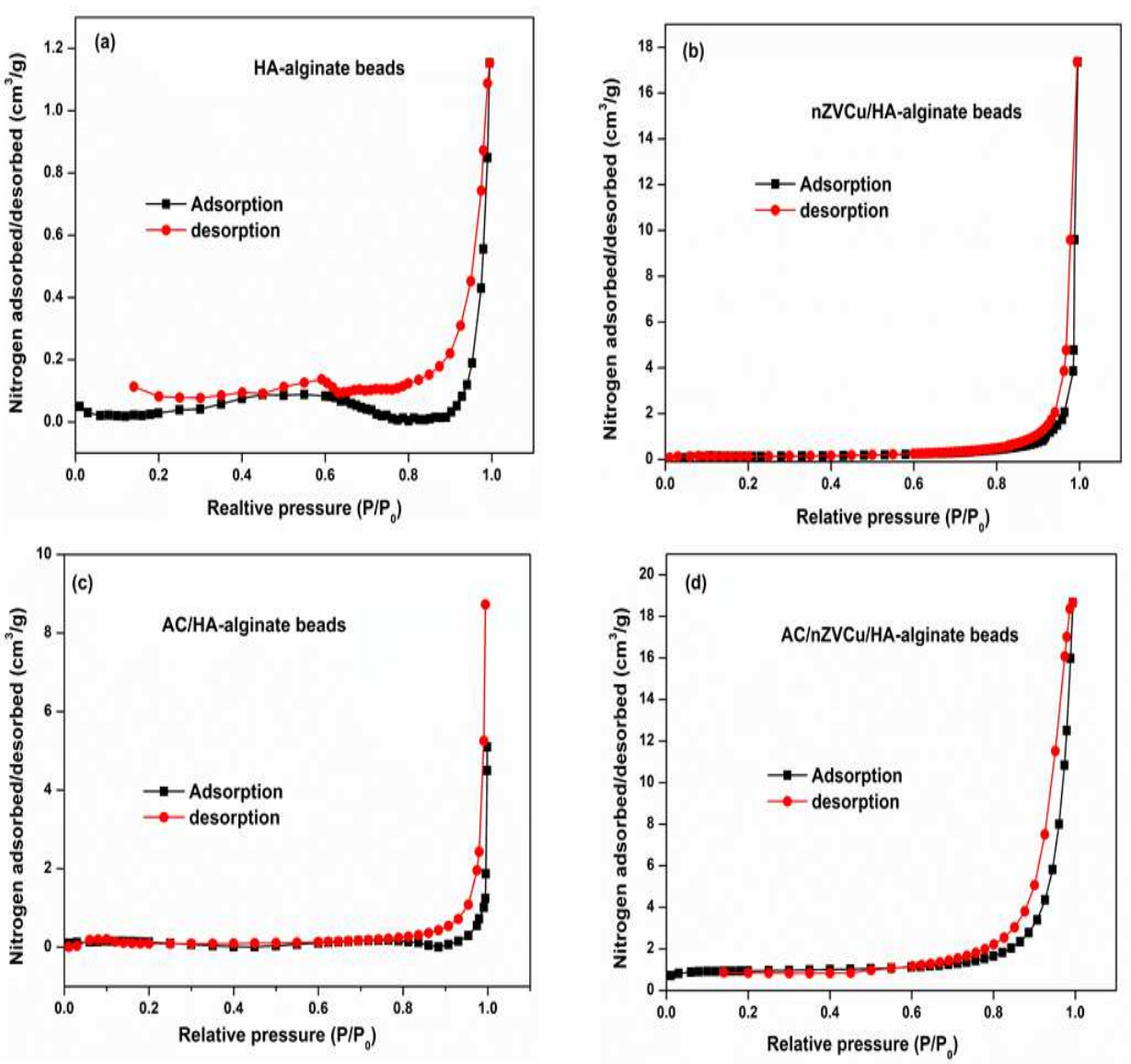
(a)
HA-alginate beads
Adsorption
desorption
Nitrogen adsorbed/desorbed (cm3/g)
Realtive pressure (P/P0)
(b)
nZVCu/HA-alginate beads
Adsorption
desorption
Nitrogen adsorbed/desorbed (cm3/g)
Relative pressure (P/P0)
(c)
AC/HA-alginate beads
Adsorption
desorption
Nitrogen adsorbed/desorbed (cm3/g)
Relative pressure (P/P0)
(d)
AC/nZVCu/HA-alginate beads
Adsorption
desorption
Nitrogen adsorbed/desorbed (cm3/g)
Relative pressure (P/P0)

Figure 1g

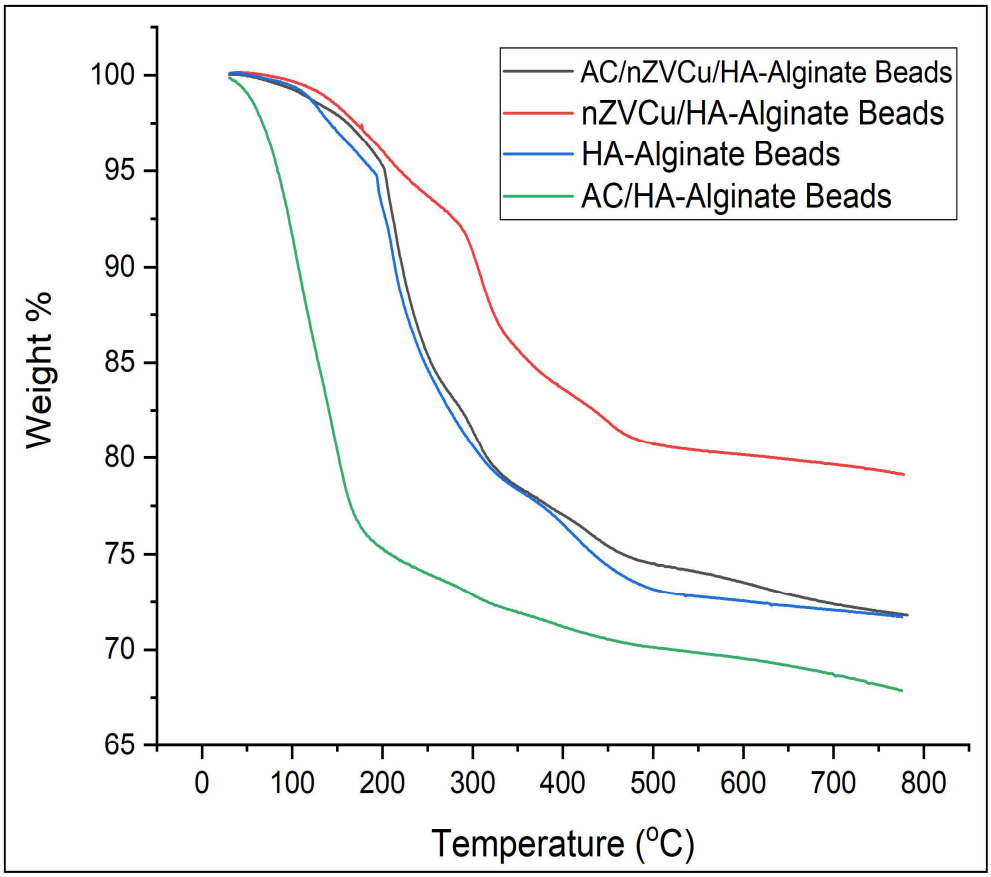

Figure 2

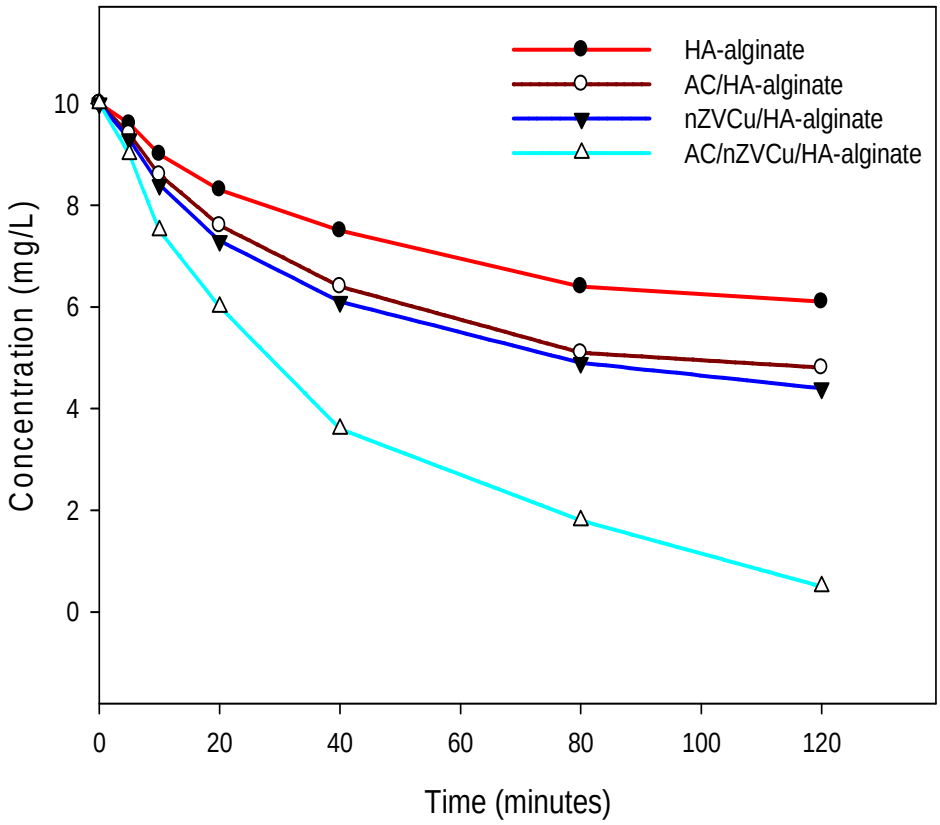

Figure 3

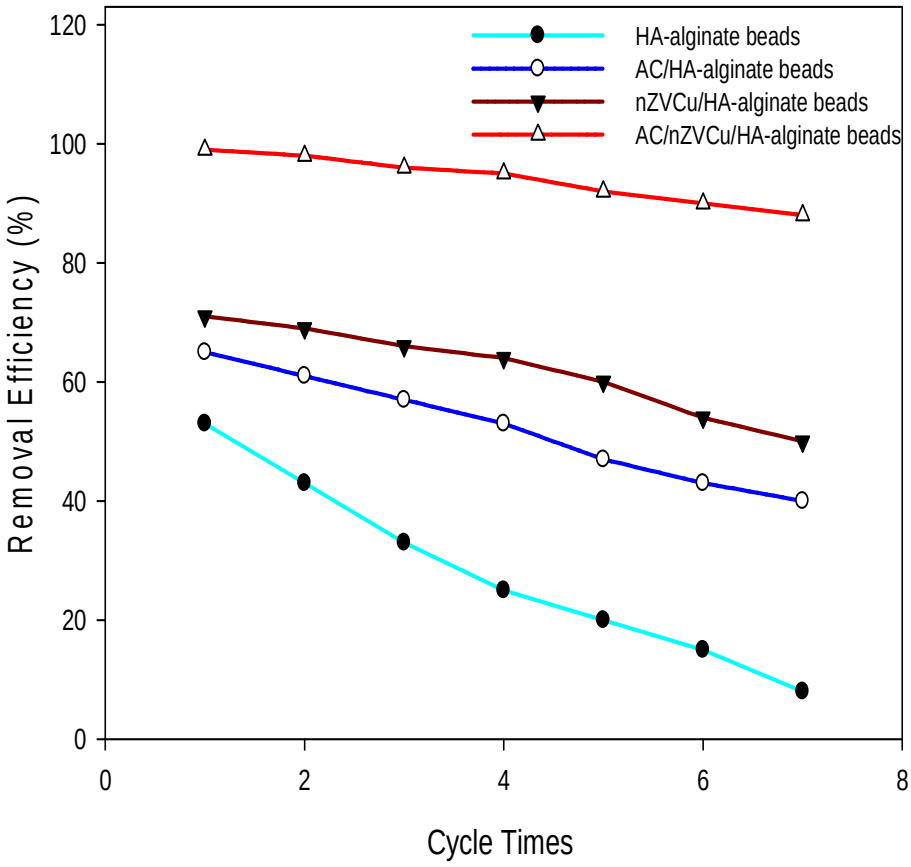
HA-alginate beads
AC/HA-alginate beads
nZVCu/HA-alginate beads
AC/nZVCu/HA-alginate beads
Removal Efficiency (%)
Cycle Times
0
20
40
60
80
100
120
0
2
4
6
8

Figure 4

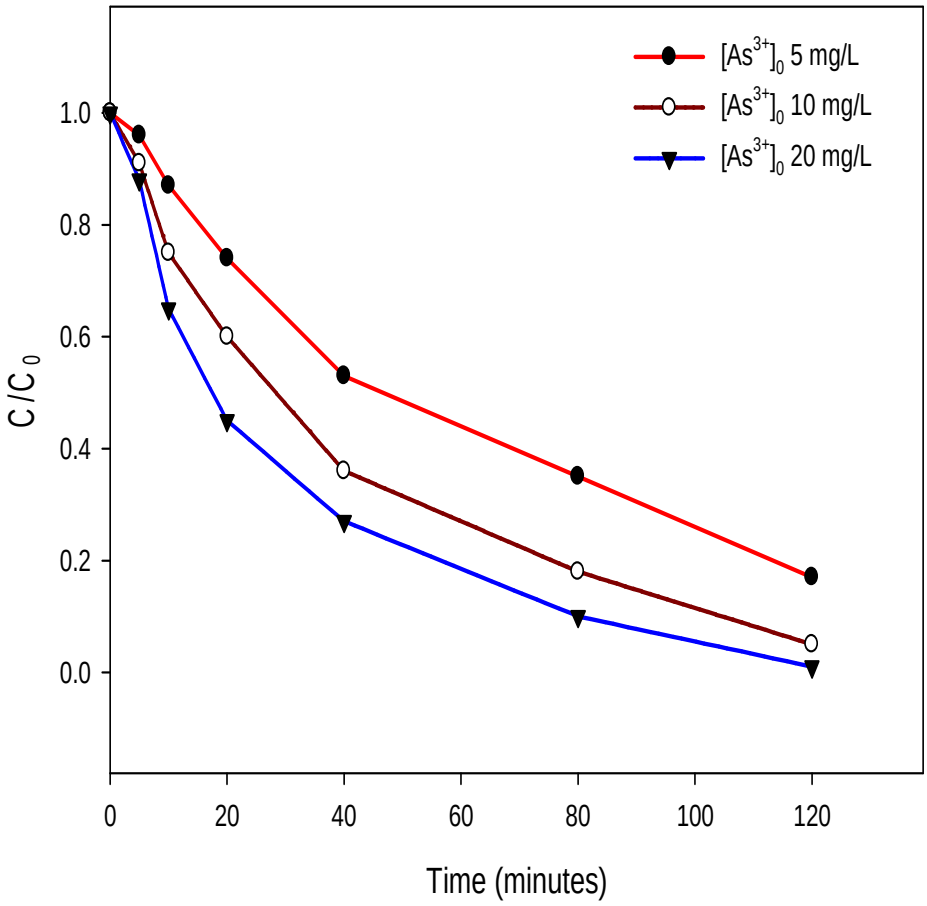
[As3+]0 5 mg/L
[As3+]0 10 mg/L
[As3+]0 20 mg/L
C/C0
1.0
0.8
0.6
0.4
0.2
0.0
0
20
40
60
80
100
120
Time (minutes)

Figure 5

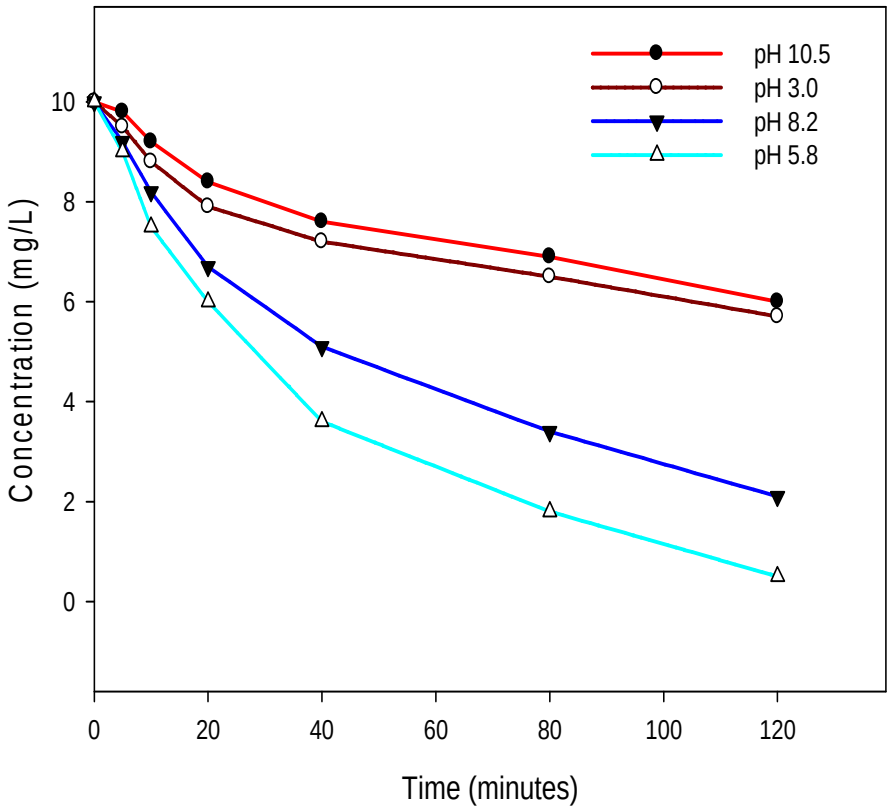

Figure 6

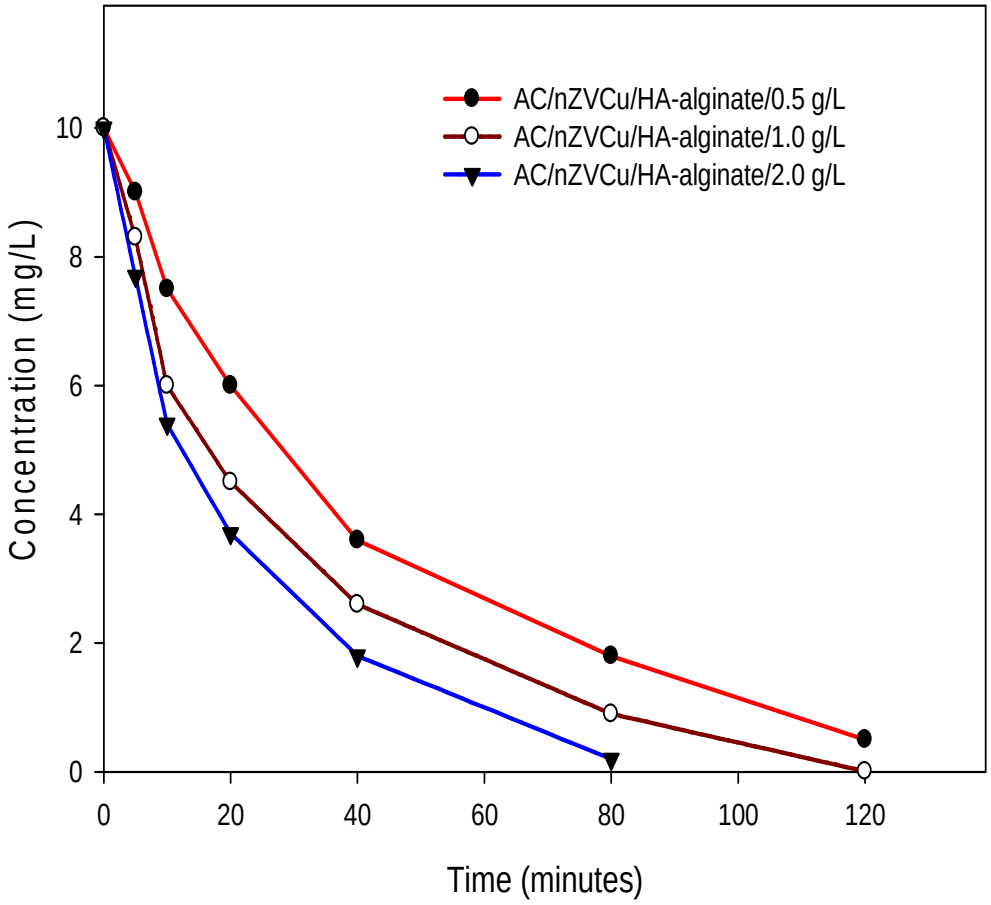

Figure 7

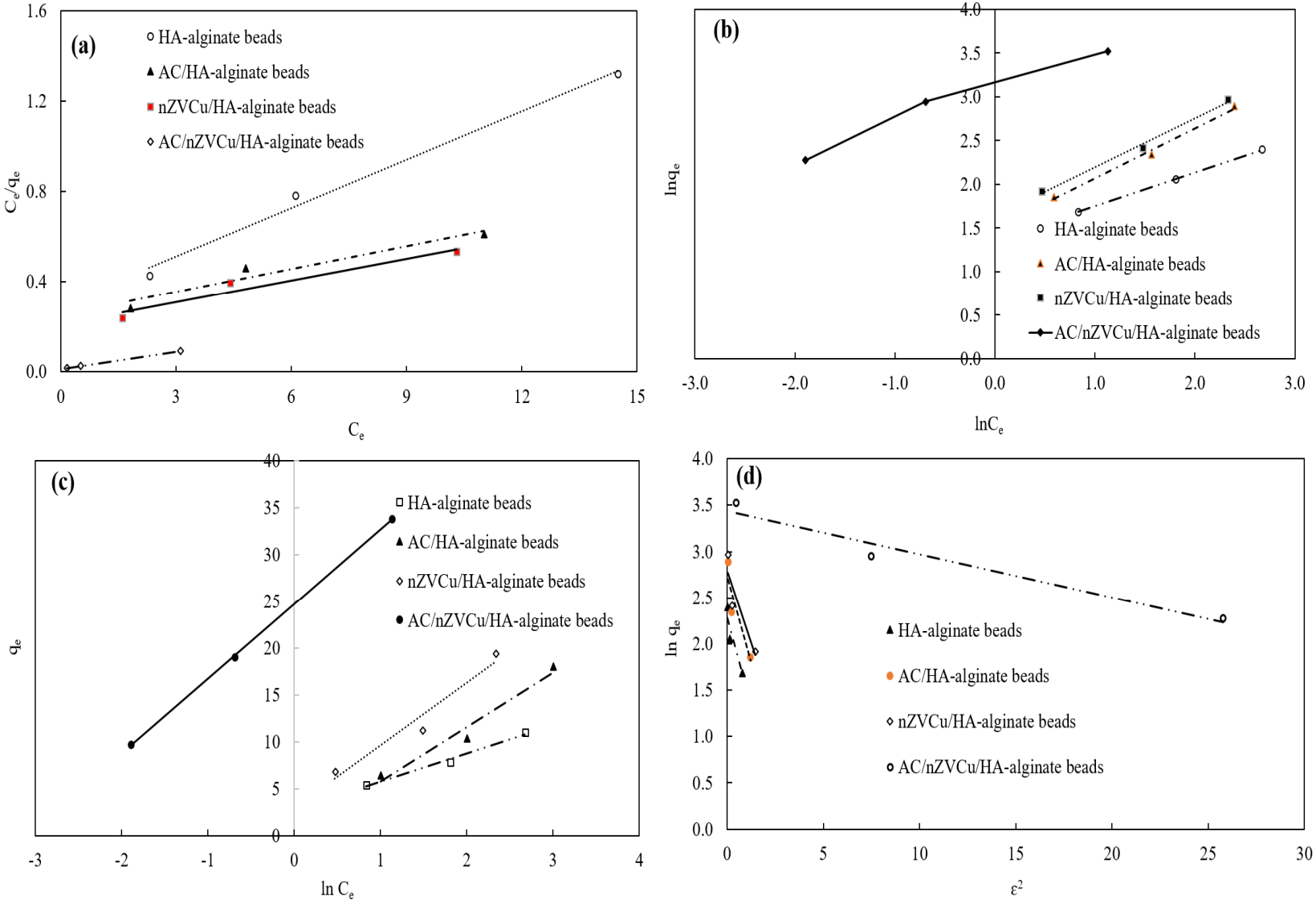
(a)
HA-alginate beads
AC/HA-alginate beads
nZVCu/HA-alginate beads
AC/nZVCu/HA-alginate beads
Ce/qe
Ce
(b)
HA-alginate beads
AC/HA-alginate beads
nZVCu/HA-alginate beads
AC/nZVCu/HA-alginate beads
lnqe
lnCe
(c)
HA-alginate beads
AC/HA-alginate beads
nZVCu/HA-alginate beads
AC/nZVCu/HA-alginate beads
qe
ln Ce
(d)
HA-alginate beads
AC/HA-alginate beads
nZVCu/HA-alginate beads
AC/nZVCu/HA-alginate beads
ln qe
ε2

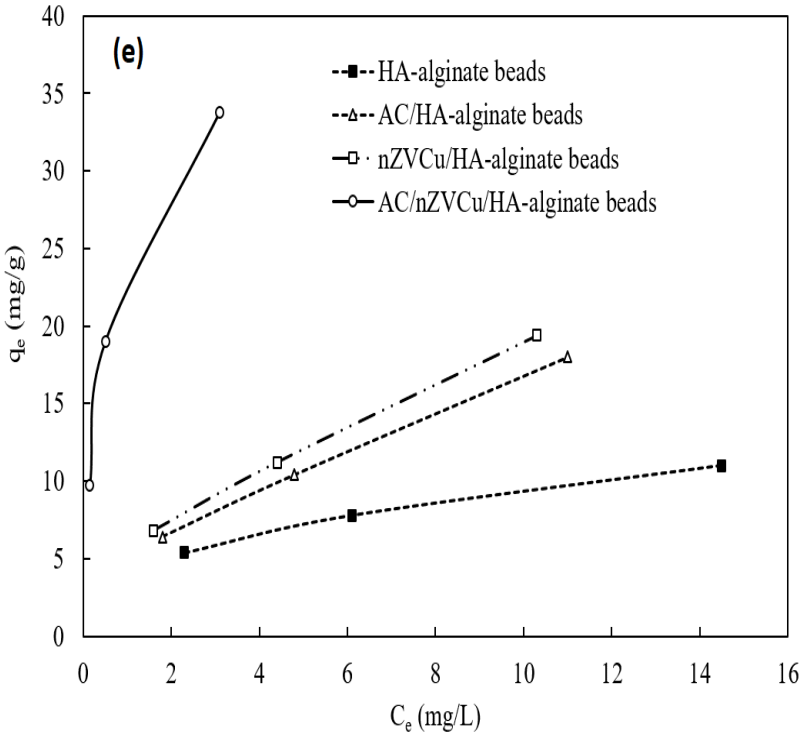

Figure 8

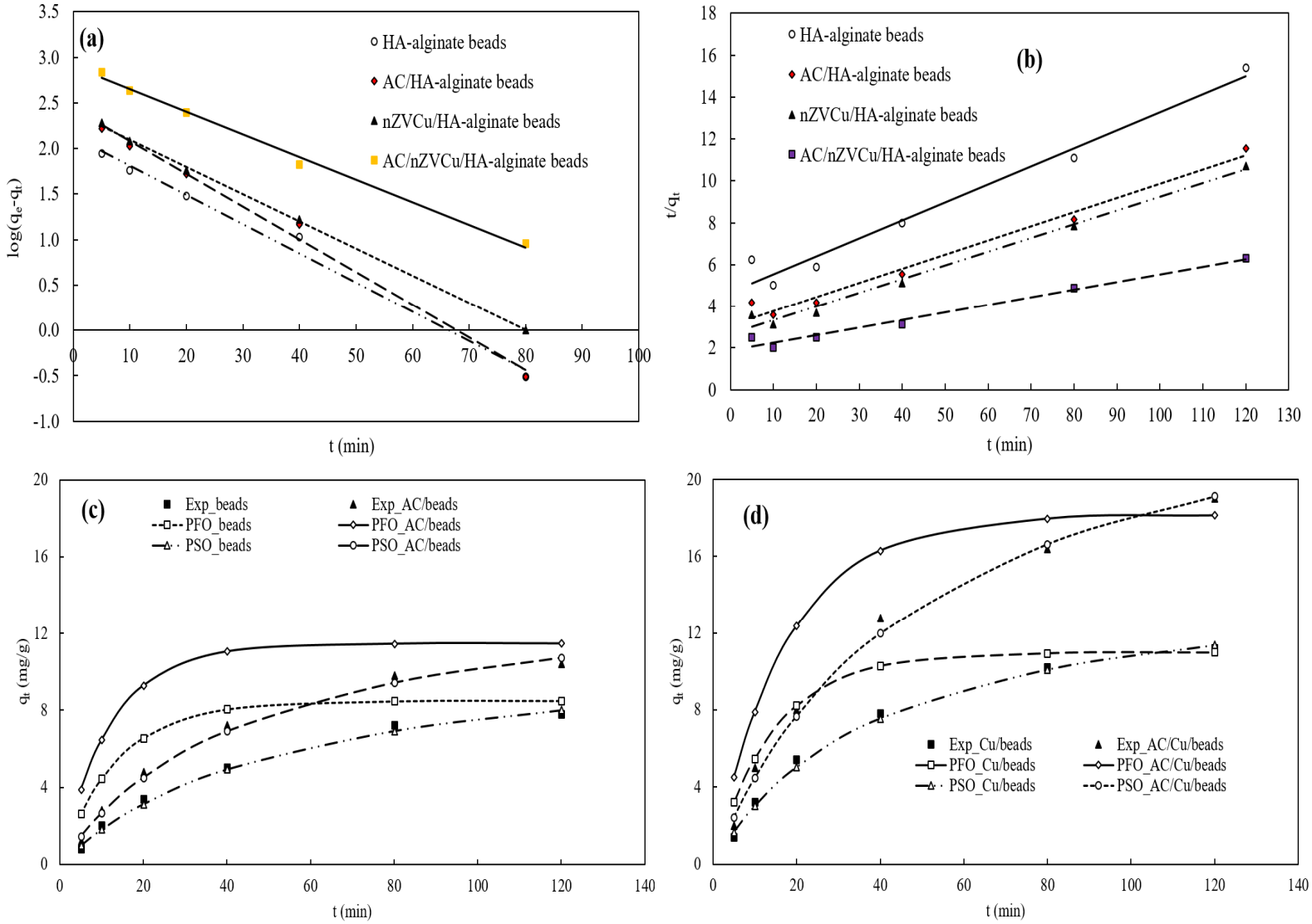
(a)
HA-alginate beads
AC/HA-alginate beads
nZVCu/HA-alginate beads
AC/nZVCu/HA-alginate beads
log(qe-qt)
t (min)
(b)
HA-alginate beads
AC/HA-alginate beads
nZVCu/HA-alginate beads
AC/nZVCu/HA-alginate beads
t/qt
t (min)
(c)
Exp_beads
Exp_AC/beads
PFO_beads
PFO_AC/beads
PSO_beads
PSO_AC/beads
qt (mg/g)
t (min)
(d)
Exp_Cu/beads
Exp_AC/Cu/beads
PFO_Cu/beads
PFO_AC/Cu/beads
PSO_Cu/beads
PSO_AC/Cu/beads
qt (mg/g)
t (min)

Table 1

Models	Parameters	HA-alginate beads	AC/HA-alginate beads	nZVCu/HA-alginate beads	AC/nZVCu/HA-alginate beads
Langmuir	K_L (L/mg)	0.24	0.13	0.15	2.05
	q_{max} (mg/g)	13.97	29.33	30.96	39.06
	R^2 (--)	0.99	0.94	0.94	0.99
Freundlich	K_F ([mg g-1(L mg-1)1/n])	3.90	4.48	5.11	22.40
	n (--)	2.59	1.76	1.78	2.47
	R^2 (--)	0.99	0.99	0.99	0.97
Temkin	K_T (L/g)	1.3×10^{6}	1.0×10^{8}	3.1×10^{6}	3.1×10^{-5}
	b (Jg/mol)	823.17	430.03	372.83	319.89
	R^2 (--)	0.99	0.97	0.95	0.99
Dubinin-Radushkevich	q_m (mg/g)	9.97	15.33	16.61	31.19
	K_{DR} (kJ/mol)	0.79	0.75	0.63	0.05
	E (kJ/mol)	0.80	0.82	0.89	3.27
	R^2 (--)	0.87	0.83	0.83	0.95
Pseudo-first-order	k_1 (1/min)	0.074	0.089	0.069	0.057
	q_e (mg/g)	8.48	11.47	11.99	18.15
	R^2 (--)	0.98	0.99	0.99	0.99
Pseudo-second-order	k_1 (g/mg/min)	0.0016	0.0015	0.0016	0.0007
	q_e (mg/g)	11.63	14.81	15.19	27.25
	R^2 (--)	0.97	0.98	0.98	0.97

Highlights

- Characterization techniques proved nZVCu and AC coupled HA-Alginate beads formation.
- Coupling AC and nZVCu enhanced performance and reusability of HA-Alginate beads.
- Removal of As^{3+} best fitted Freundlich isotherm and *pseudo-first-order* models.
- Removal of As^{3+} was significantly affected by the pH of aqueous solution.